Shixuan Yang
Center for Mechanics of Solids, Structures, and Materials,
Department of Aerospace Engineering and Engineering Mechanics,
The University of Texas at Austin,
210 E 24th Street,
Austin, TX 78712

Shutao Qiao
Center for Mechanics of Solids, Structures, and Materials,
Department of Aerospace Engineering and Engineering Mechanics,
The University of Texas at Austin,
210 E 24th Street,
Austin, TX 78712

Nanshu Lu[1]
Center for Mechanics of Solids, Structures, and Materials,
Department of Aerospace Engineering and Engineering Mechanics,
The University of Texas at Austin,
210 E 24th Street,
Austin, TX 78712;
Department of Biomedical Engineering,
The University of Texas at Austin,
107 W Dean Keeton St.,
Austin, TX 78712;
Texas Materials Institute,
The University of Texas at Austin,
204 E. Dean Keeton St.,
Austin, TX 78712
e-mail: nanshulu@utexas.edu

Elasticity Solutions to Nonbuckling Serpentine Ribbons

Stretchable electronics have found wide applications in bio-mimetic and bio-integrated electronics attributing to their softness, stretchability, and conformability. Although conventional electronic materials are intrinsically stiff and brittle, silicon and metal membranes can be patterned into in-plane serpentine ribbons for enhanced stretchability and compliance. While freestanding thin serpentine ribbons may easily buckle out-of-plane, thick serpentine ribbons may remain unbuckled upon stretching. Curved beam (CB) theory has been applied to analytically solve the strain field and the stiffness of freestanding, nonbuckling serpentine ribbons. While being able to fully capture the strain and stiffness of narrow serpentines, the theory cannot provide accurate solutions to serpentine ribbons whose widths are comparable to the arc radius. Here we report elasticity solutions to accurately capture nonbuckling, wide serpentine ribbons. We have demonstrated that weak boundary conditions are sufficient for solving Airy stress functions except when the serpentine's total curve length approaches the ribbon width. Slightly modified weak boundary conditions are proposed to resolve this difficulty. Final elasticity solutions are fully validated by finite element models (FEM) and are compared with results obtained by the curved beam theory. When the serpentine ribbons are embedded in polymer matrices, their stretchability may be compromised due to the fact that the matrix can constrain the in-plane rotation of the serpentine. Comparison between the analytical solutions for freestanding serpentines and the FEM solutions for matrix-embedded serpentines reveals that matrix constraint remains trivial until the matrix modulus approaches that of the serpentine ribbon. [DOI: 10.1115/1.4035118]

Keywords: stretchable electronics, serpentine, elasticity, stretchability, stiffness

1 Introduction

Since its emergence in the mid-2000's, stretchable electronics [1,2] has found many exciting applications including bio-mimetic electronics such as electronic skin [3] and hemispherical electronic eye camera [4], bio-integrated electronics represented by epidermal electronics [5] and bioresorbable soft brain sensors [6], as well as stretchable energy sources exemplified by organic solar cells [7] and rechargeable batteries [8]. Although many electronic materials are intrinsically stiff and even brittle, they can still be included in stretchable electronics thanks to various strain-relieving structural designs. For example, the mechanics of wrinkled or buckled stiff membranes or ribbons on compliant substrates [9–11] has enabled stretchable gold conductors [12], silicon transistors [13], organic solar cells [7], lead zirconate titanate (PZT) generators [14], as well as graphene strain gauges [15].

As buckled structures cannot be easily encapsulated or integrated with bio-tissues, a more popular design in recent years is to pattern stiff membranes into in-plane meandering ribbons which are often called serpentines [16–20]. Serpentine structures can effectively convert in-plane and out-of-plane bending to significant end-to-end extension without inducing large strains in the material. In stretchable electronics, serpentine designs were initially implemented for stretchable metallic interconnects [16–18,20], sometimes between isolated rigid device islands [19,21]. Later, graphene [22], zinc oxide (ZnO) [23], indium tin oxide (ITO) [24], and conductive elastomer [25]-based serpentines have emerged. Eliminating the device islands and patterning gold and silicon into filamentary serpentine network has enabled epidermal electronics [5], whose stretchability and softness are well matched with human skin. Fractal serpentine design leverages ordered unraveling of self-similar serpentine designs to concurrently achieve high areal coverage and large stretchability [26,27]. While substrate-bonded thin film serpentines are often found in stretchable electronics, freestanding thick serpentine ribbons are often used in expandable or deployable structures. For example, conventional or smart cardiovascular stents with metal serpentine skeletons [28] can remain small radius during insertion through blood vessels and expand for angioplasty once in place. As another example, ultra-narrow, accordion-like freestanding polyimide serpentines were designed to form a spider-web-like highly expandable micro-sensor network that can cover giant aerospace structures [29]. It is well known that when stretched, thin serpentines can easily buckle out-of-plane as out-of-plane bending consumes less energy than in-plane bending. However, when the serpentine is thick enough (i.e., when thickness is larger than ribbon width), in-plane bending becomes more energetically favorable than out-of-plane bending. As a result, thick serpentines can be stretched without buckling.

The mechanics of serpentines has been under active investigations in recent years. On the one hand, quite a few analysis have been conducted to study the buckling and post-buckling behaviors of freestanding serpentine ribbons of basic shapes [17,30–32] as well as self-similar ones [27,33,34]. On the other hand, mechanics

[1]Corresponding author.

Contributed by the Applied Mechanics Division of ASME for publication in the Journal of Applied Mechanics. Manuscript received September 13, 2016; final manuscript received October 31, 2016; published online November 17, 2016. Editor: Yonggang Huang.

of polymer-embedded or polymer-bonded serpentines are mostly studied through combined experimental and finite element modeling (FEM) means [16,20,24,35–39]. We have obtained closed-form linear elasticity solutions for freestanding, nonbuckling serpentine structures through curved beam (CB) theory [40], which is well validated by experiments and FEM on narrow, filamentary serpentine ribbons.

Although narrow serpentines are known to be more stretchable than wide ones, serpentine width can be limited by practical factors. For example, the lower bound of serpentines width is set by the resolution of the patterning technology, which can be hundreds of microns for some popular low-cost manufacturing methods such as screen printing [41] or mechanical cutting [42]. In applications such as stretchable photovoltaics and epidermal electrodes, large areal coverage is critical and therefore wider serpentines may improve device functionality. However, when comparing the strain field of wide serpentines obtained by CB theory and by FEM, we found significant deviations. This can be attributed to the essential assumption in CB theory that cross-sectional planes remain planar after deformation. As a result, in this paper, we apply elasticity theory to derive analytical solutions for nonbuckling serpentines of all widths. The strain and stiffness results are fully validated by FEM.

2 Analytical Modeling

The problem we intend to study is a periodic serpentine ribbon subjected to uniaxial stretch. A 3D schematic of the unit cell is depicted in Fig. 1(*a*), where the curved section is named the *arc*, and the linear section is named the *arm*. The out-of-plane thickness is t, and the in-plane geometry of the serpentine ribbon can be fully defined by four independent parameters: the arc radius R, the ribbon width w, the arm length l, and the arc opening angle α. After nondimensionalization, three independent dimensionless geometric parameters will be used in this study: w/R, l/R, and α. These parameters are essentially the three degrees of freedom in the 3D serpentine design space as illustrated in Fig. 1(*b*). Different serpentine geometries can be defined by different combinations of the three parameters, which can be represented as points in the first and the fifth quadrants of this 3D design space. A uniaxial tensile displacement u_0 in the direction of periodicity is applied at each end of this unit cell as indicated in Fig. 1(*a*). As we limit ourselves to ribbons that do not buckle out-of-plane under applied displacement u_0, plane strain condition can be assumed such that we only need to solve a 2D elasticity problem. If we define *applied strain* to be the strain induced by u_0 in the linear counterpart of the serpentine ribbon, the applied strain can be expresses as

$$\varepsilon_{\text{app}} = \frac{2u_0}{S} \tag{1}$$

where S represents the initial length of the linear counterpart, i.e., the initial end-to to-end distance of the serpentine unit cell

$$S = 4\left(R\cos(\alpha) - \frac{l}{2}\sin(\alpha)\right) \tag{2}$$

Attributing to the symmetric and anti-symmetric features of the serpentine structure as well as the load and boundary conditions, the unit cell can be further reduced to a quarter cell as illustrated in Fig. 1(*b*). Specifically, the right end of the quarter cell is set to be symmetric boundary condition. A displacement of $u_0/2$ is applied at the middle point of the left end, whose reaction force is denoted by P. In the follows, we will derive P, stress and strain fields as functions of u_0 and serpentine geometry using elasticity theory and will compare the elasticity results with our previous CB solutions [40].

In the context of stretchable electronics, we are particularly interested in two mechanical behaviors of serpentines: the stretchability and the effective stiffness. *Stretchability* is defined as the critical applied strain beyond which the serpentine ribbon ruptures and is denoted by $\varepsilon_{\text{app}}^{\text{cr}}$. Therefore, if the failure criterion is $\varepsilon_{\max} = \varepsilon_{\text{cr}}$, where $\varepsilon_{\max}$ and ε_{cr} represent the maximum tensile strain in the serpentine ribbon and the critical strain-to-rupture or strain-to-yield of the material, respectively, the normalized maximum tensile strain in the serpentine, $\varepsilon_{\max}/\varepsilon_{\text{app}}$, will govern the stretchability through

$$\varepsilon_{\text{app}}^{\text{cr}} = \frac{\varepsilon_{\text{cr}}}{\varepsilon_{\max}/\varepsilon_{\text{app}}} \tag{3}$$

Effective stiffness is defined as the ratio of the reaction force P to the end-to-end displacement. With Young's modulus E and Poisson's ratio ν, the stiffness of a plane strain (t assumed to be 1) linear ribbon of length S and width w is given by $\bar{E}w/S$, where $\bar{E} = E/(1-\nu^2)$ is the plane strain modulus. Therefore, the effective stiffness of a serpentine ribbon normalized by that of its linear counterpart is given by $PS/(2\bar{E}wu_0)$. When α approaches $-\pi/2$, i.e., when the serpentine degenerates to a linear ribbon, both $\varepsilon_{\max}/\varepsilon_{\text{app}}$ and $PS/(2\bar{E}wu_0)$ should approach one.

The goal of this paper is to use elasticity to derive $\varepsilon_{\max}/\varepsilon_{\text{app}}$ and $PS/(2\bar{E}wu_0)$ as functions of the three dimensionless geometric parameters w/R, l/R, and α. Airy stress function is a classical approach to tackle 2D elasticity problem. For derivation, we decompose the original boundary value problem (BVP) shown in Fig. 1(*c*) into three sub-BVPs, as illustrated in Figs. 2(*a*)–2(*c*). Figures 2(*a*) and 2(*b*) depict two sub-BVPs for the arc, where M_2 in Fig. 2(*a*) is the moment that balances P in the arc section. M_1 in Fig. 2(*c*) is the moment that balances P in the arm section, and M_1 in Fig. 2(*b*) is the reaction moment. Hence, we obtain

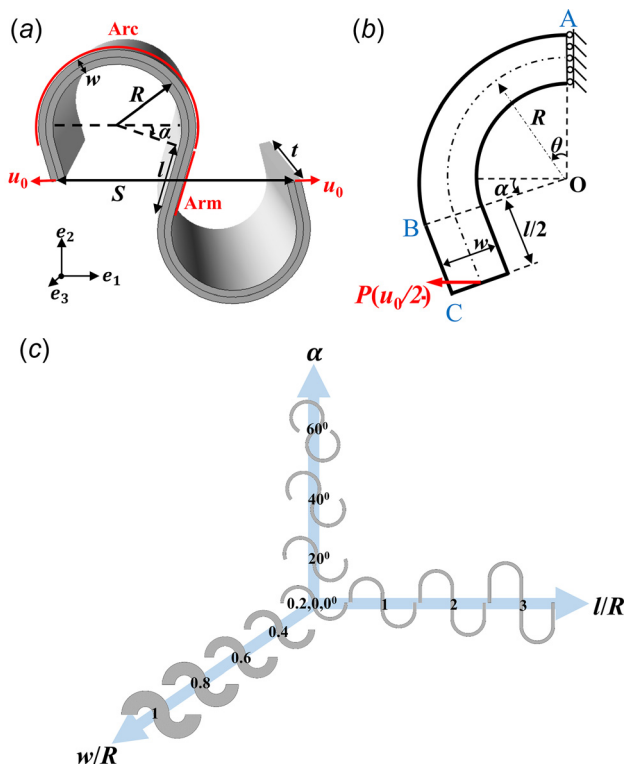

Fig. 1 (*a*) Three-dimensional schematic of the unit cell of a freestanding periodic serpentine ribbon with geometric parameters and boundary conditions labeled. (*b*) Simplified plane strain boundary value problem (BVP) of a nonbuckling serpentine ribbon. (*c*) The three-dimensional design space for serpentine shapes defined by three dimensionless geometric parameters.

$$M_1 = P\frac{l}{2}\cos(\alpha) \tag{4}$$

$$M_2 = P\frac{a+b}{2}(1+\sin(\alpha)) \tag{5}$$

where a and b represent the inner and outer radii of the arc

$$a = R - \frac{w}{2}, b = R + \frac{w}{2} \tag{6}$$

The resultant moment M at the fixed end of the arc is therefore given by

$$M = M_1 + M_2 \tag{7}$$

The original BVP is now decomposed into three sub-BVPs with simple geometry and well-defined boundary conditions and it is hence possible to find corresponding Airy stress functions for each of them. Polar coordinate system is adopted to solve the stress/strain field in the arc whereas Cartesian coordinate system is used for the arm, as illustrated in Figs. 2(*a*)–2(*c*). Three Airy stress functions can be constructed for the sub-BVPs defined in Figs. 2(*a*), 2(*b*), and 2(*c*), respectively

$$\varphi_1 = \left(\frac{A_1}{r} + A_2\ r\ln(r) + A_3\ r^3\right)\cos(\theta) + A_4\ln(r) + A_5 r^2 + A_6 r^2\ln(r) \tag{8}$$

$$\varphi_2 = B_1\ \ln(r) + B_2\ r^2 + B_3\ r^2\ \ln(r) \tag{9}$$

$$\varphi_3 = C_1\ y^2 + C_2\ xy + C_3 y^3 + C_4 xy^3 \tag{10}$$

where As, Bs, and Cs are constants to be determined by boundary conditions.

The stress field for each of the sub-BVPs can then be derived by taking derivatives of the corresponding stress function in polar or Cartesian coordinate and can be expressed in terms of geometrical parameters, applied force P, spatial variables (r, θ) or (x, y), and the unknown constants. The unknown constants can be determined by implementing weak force boundary conditions:

For Fig. 2(*a*)

$$\begin{cases} 1.\ r = a,\ \ \sigma_{rr} = \sigma_{r\theta} = 0 \\ 2.\ r = b, \sigma_{rr} = \sigma_{r\theta} = 0 \\ 3.\theta = 0, \int_a^b \sigma_{\theta\theta} dr = P, \int_a^b \sigma_{r\theta} dr = 0, \int_a^b \sigma_{\theta\theta} r dr = \left(\frac{a+b}{2} + c\right) P\sin(-\alpha) \\ 4.\quad \theta = \frac{\pi}{2} + \alpha, \int_a^b \sigma_{\theta\theta} dr = P\sin(-\alpha), \int_a^b \sigma_{r\theta} dr = P\cos(\alpha), \int_a^b \sigma_{\theta\theta} r dr = \left(\frac{a+b}{2} + c\right) P\sin(-\alpha) \end{cases} \tag{11}$$

where c is an offset that will be discussed later.

For Fig. 2(*b*)

$$\begin{cases} 1.\ r = a,\ \ \sigma_{rr} = \sigma_{r\theta} = 0 \\ 2.\ r = b, \sigma_{rr} = \sigma_{r\theta} = 0 \\ 3.\theta = 0, \int_a^b \sigma_{\theta\theta} dr = 0, \int_a^b \sigma_{r\theta} dr = 0, \int_a^b \sigma_{\theta\theta} r dr = -\frac{l}{2} P\cos(\alpha) \\ 4.\quad \theta = \frac{\pi}{2} + \alpha, \int_a^b \sigma_{\theta\theta} dr = 0, \int_a^b \sigma_{r\theta} dr = 0, \int_a^b \sigma_{\theta\theta} r dr = -\frac{l}{2} P\cos(\alpha) \end{cases} \tag{12}$$

For Fig. 2(*c*)

$$\begin{cases} 1.y = -\frac{b-a}{2}, \sigma_{yy} = \sigma_{xy} = 0 \\ 2.y = \frac{b-a}{2}, \sigma_{yy} = \sigma_{xy} = 0 \\ 3.x = 0, \int_{-\frac{b-a}{2}}^{\frac{b-a}{2}} \sigma_{xx} dy = P\sin(-\alpha), \int_{-\frac{b-a}{2}}^{\frac{b-a}{2}} \sigma_{xy} dy = -P\ \cos(\alpha), \int_{-\frac{b-a}{2}}^{\frac{b-a}{2}} \sigma_{xx}(y+c) dy = \frac{l}{2} P\cos(\alpha) \\ 4.\quad x = \frac{l}{2}, \int_{-\frac{b-a}{2}}^{\frac{b-a}{2}} \sigma_{xx} dy = P\sin(-\alpha), \int_{-\frac{b-a}{2}}^{\frac{b-a}{2}} \sigma_{xy} dy = -P\ \cos(\alpha), \int_{-\frac{b-a}{2}}^{\frac{b-a}{2}} \sigma_{xx}(y+c) dy = 0 \end{cases} \tag{13}$$

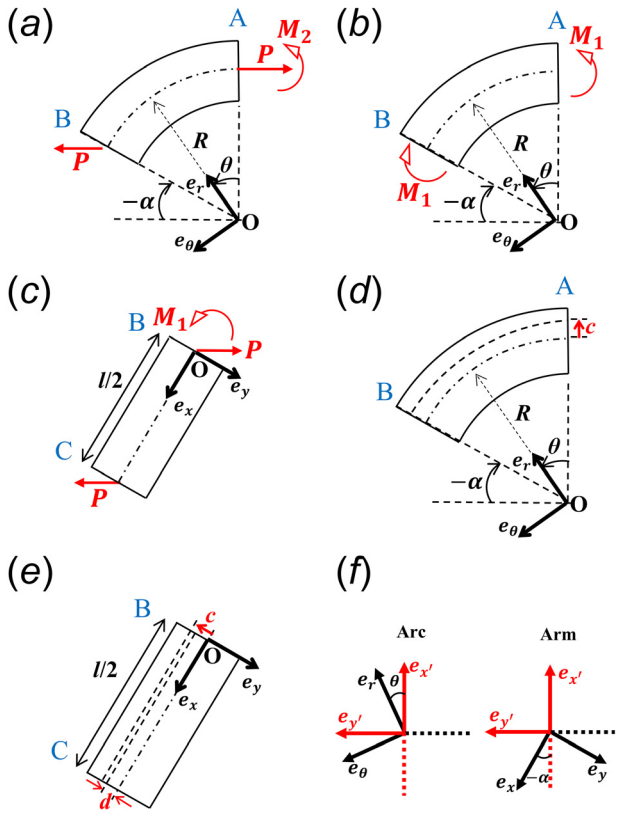

Fig. 2 Boundary conditions for three decomposed sub-BVPs: (*a*) and (*b*) are two sub-BVPs for the arc and (*c*) is for the arm. (*d*) Definition of the *c* offset. (*e*) Definition of the *d* offset. (*f*) Illustration of the local and global coordinate systems.

Those weak boundary conditions would fail when α approaches $-\pi/2$ and in the meanwhile, l approaches 0. When the arm length l is 0, the serpentine comprises only the arc. Independently, when the arc opening angle α approaches $-\pi/2$, the serpentine approaches a straight beam almost without an arc. Therefore, the configuration of $\alpha \to -\pi/2$ and $l \to 0$ describes a nearly straight ribbon with very small total length. In this scenario, the total curve length of the serpentine approaches 0, which may be even smaller than the ribbon width. Under this situation, the Saint-Venant's principle no longer holds. Violation of the Saint-Venant's principle implies the weak boundary condition is no longer applicable. One way to resolve this issue is to apply point-wise boundary condition to solve the stress functions, which may lead to excessively complicated solution. Another approach is to make minimum modification to the solution based on weak boundary conditions, which will result in relatively succinct solution. We therefore take the second approach and assume that the reaction force P is not applied right at the median line of the ribbon, but with an offset of c, as illustrated in Figs. 2(*d*) and 2(*e*). c can be solved semi-analytically as discussed later. After obtaining the stress functions, the stress field can be solved accordingly and is offered in Eqs. (A1)–(A3) in the Appendix. Applying the plane strain constitutive law, strain field can also be obtained. Both stress and strain solutions contain the unknown reaction force, P, which has to be solved as a function of the applied displacement. And the displacement field can be solved by the geometric equations, with the following boundary and continuity conditions:

$$\begin{cases} 1.\, u_{\text{arm}|x=0,y=-\text{d}} = 0 \\ 2.\, v_{\text{arm}|x=0,y=-\text{d}} = 0 \\ 3.\, \phi_{\text{arm}|x=0,\ y=-\text{d}} = \phi_{\text{arc}|r=\dfrac{a+b}{2}+\text{d},\,\theta=\dfrac{\pi}{2}+\alpha} \end{cases} \tag{14}$$

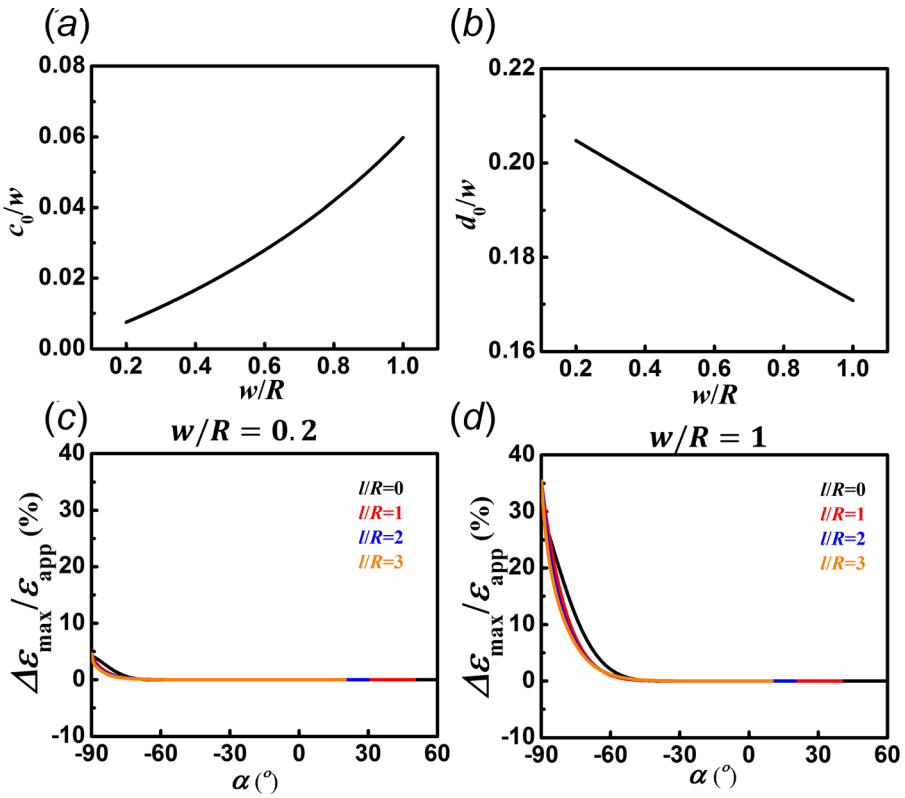

Fig. 3 The normalized offsets when $\alpha = -\pi/2$: (*a*) c_0/w and (*b*) d_0/w analytically solved as functions of w/R. Difference in $\varepsilon_{max}/\varepsilon_{app}$ with and without the offsets for (*c*) narrow serpentines ($w/R = 0.2$) and (*d*) wide serpentines ($w/R = 1$).

where u and v are the displacements and ϕ stands for the rotation. The continuity condition is in a weak form that only the point defined by $x = 0,\ y = -d$ has continuous displacement and rotation. The d offset in the arm is illustrated in Fig. 2(*e*), which will be solved semi-analytically later. The final displacement solution is offered in Eqs. (A4) and (A5) in the Appendix.

So far, the stress, strain, and displacement are all derived in the local polar or local Cartesian coordinates. To obtain results in the global Cartesian coordinate, one more step of coordinate transformation has to be implemented. The global coordinates $\{\boldsymbol{e}_{x'}, \boldsymbol{e}_{y'}\}$ along with the local coordinates $\{e_x, e_y\}$ are illustrated in Fig. 2(*f*) and the transformation angle for arc and arm are

$$\phi_1 = -\theta \text{ and } \phi_2 = -(\pi + \alpha) \tag{15}$$

respectively.

Through coordinate transformation, the displacement results can be expressed in the global Cartesian coordinate as u' (displacement in $\boldsymbol{e}_{x'}$ direction) and v' (displacement in $\boldsymbol{e}_{y'}$ direction). The applied displacement is finally linked to the applied force P through

$$u_{\text{app}} = \frac{u_0}{2} = v'_{\text{arc}|r=\frac{a+b}{2}+d,\theta=\frac{\pi}{2}+\alpha} + v'_{\text{arm}|x=\frac{l}{2},y=0} \tag{16}$$

Given applied strain defined in Eq. (2), we want to solve for the maximum strain in the serpentine, which dictates the stretchability of the serpentine. As previous study on nonbuckling serpentines [40] suggests that the maximum strain always occurs at the inner crest of the arc, we can find the maximum strain as

$$\varepsilon_{\max} = \varepsilon_{\theta}^{\text{arc}|r=a,\theta=0} \tag{17}$$

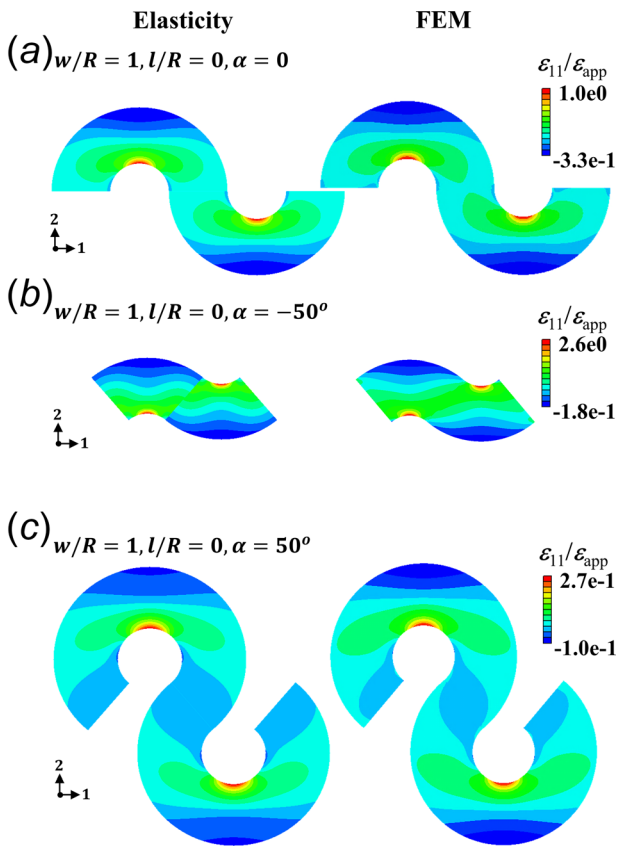

Fig. 4 Comparison of strain field obtained by elasticity theory (left frames) and FEM (right frames) for serpentines with geometric parameters (*a*) $w/R = 1,\ l/R = 0, \alpha = 0$, (*b*) $w/R = 1,\ l/R = 0, \alpha = -50$ *deg*, and (*c*) $w/R = 1,\ l/R = 0, \alpha = 50$ deg

Therefore, $\varepsilon_{\max}/\varepsilon_{\text{app}}$ can be written as a function $f(w/R, l/R, \alpha, \nu)$ and, $PS/(2\bar{E}wu_0)$ as a function of $g(w/R, l/R, \alpha, \nu)$. Offsets c and d are just functions of the geometric parameters $(w, R,\ l,\ \alpha)$. If we define $c_0 = c(w,\ R,\ l \to 0,\ \alpha \to -\pi/2)$ and $d_0 = d(w,\ R,\ l \to 0,\ \alpha \to -\pi/2)$, c_0 and d_0 can be solved by setting $\varepsilon_{\max}/\varepsilon_{\text{app}} = 1$ and $PS/(2\bar{E}wu_0) = 1$ when $l \to 0$ and $\alpha \to -\pi/2$. Figures 3(*a*) and 3(*b*) plot c_0/w and d_0/w as functions of w/R, respectively. It is obvious that c_0/w increases with increasing w/R while d_0/w decreases with increasing w/R. As we pointed out before, when α grows from $-\pi/2$, the effect of weak boundary conditions on the stress field decays; thus, c and d should vary with α. Simply assuming 4th order dependence, we propose the full solutions to be

$$c = \begin{cases} c_0\left(\dfrac{2\alpha}{\pi}\right)^4 & \alpha \le 0 \\ 0 & \alpha > 0 \end{cases},\quad d = \begin{cases} d_0\left(\dfrac{2\alpha}{\pi}\right)^4 & \alpha \le 0 \\ 0 & \alpha > 0 \end{cases} \tag{18}$$

where the 4th power was assumed such that c and d can decay drastically as α departs from $-\pi/2$.

To explain the importance of the two offsets, Figs. 3(*c*) and 3(*d*) plot the difference in $\varepsilon_{\max}/\varepsilon_{\text{app}}$ with and without considering them, for narrow serpentines ($w/R = 0.2$) and wide serpentines ($w/R = 1$), respectively. Both figures indicate that the effect of c and d becomes more significant as α approaches $-\pi/2$, where the weak boundary conditions break down, and is negligible when α is big. Comparing Fig. 3(*c*) with Fig. 3(*d*), it is obvious that including the offsets is more important for wider serpentines.

Finally, we can obtain elasticity solutions for $\varepsilon_{\max}/\varepsilon_{\text{app}} = f(w/R, l/R, \alpha,\ \nu)$ and $PS/(2\bar{E}wu_0) = g(w/R, l/R, \alpha,\ \nu)$ using MATHEMATICA, and the code is supplied in (See Supplemental results which are available under "Supplemental Materials" tab for this paper on the ASME Digital Collection.)

3 Results and Discussion

3.1 Strain in Serpentine Ribbons. As the elasticity solutions are difficult to express analytically, we will use contour plots and graphs to illustrate the strain results. Figure 4 compares the ε_{11} distribution solved by elasticity (left frames) with those solved by FEM (right frames) for various serpentine shapes. It is obvious that the results agree well with each other except when the serpentine is short and wide (e.g., Fig. 3(*b*)), which is due to the introduction of the offsets. In all cases, the maximum strains always occur at the inner crest of the arc and are very similar when comparing the elasticity and FEM solutions.

To compare FEM, CB, and elasticity solutions altogether, Figs. 5(*a*)–5(*d*) plot the normalized maximum strain $\varepsilon_{\max}/\varepsilon_{\text{app}}$ as dots for FEM results, dashed curves for CB solutions, and solid curves for elasticity solutions. Insets in each plot depict representative serpentine shapes pertinent to that plot with the x variable labeled beneath the shape. Figure 5(*a*) plots $\varepsilon_{\max}/\varepsilon_{\text{app}}$ as a function of w/R with varying l/R (represented by curve colors) but fixed α ($\alpha = 0$, i.e., arcs are half circles). The black curve represents the elasticity solution for serpentine ribbons with $\alpha = 0$ and $l/R = 0$, which is identical to the elasticity solution to this shape in our previous paper on CB solutions [40]. FEM, CB, and elasticity results all indicate that $\varepsilon_{\max}/\varepsilon_{\text{app}}$ increases monotonically with increasing w/R, which is expected because the inner crest of the arc of wider serpentines should experience stronger bending-induced tensile strain when the serpentine is stretched end to end. It is also consistent among the three results that serpentines with longer arms (larger l/R) have lower maximum strains, which is because the rigid body rotation of the long arm can help accommodate the applied displacement. Comparing the three different types of solutions, Fig. 5(*a*) suggests that CB theory is only valid when w/R is small, which is attributed to the failure of the CB assumption when the ribbon gets too wide. We also notice that the deviation between CB and FEM can be delayed when l/R is large, i.e.,

serpentines with longer total curve length. In contrast, elasticity solution always perfectly predicts FEM results, for large and small w/R. Figure 5(*b*) plots the same results as Fig. 5(*a*) with l/R being the x-axis and w/R in different colors. It is more obvious here that $\varepsilon_{max}/\varepsilon_{app}$ decays monotonically with increasing l/R, which means serpentines with longer arms can yield higher stretchability. We can also conclude from Fig. 5(*b*) that CB theory is more applicable to serpentines with longer arms where arm rotation instead of arc bending is the main stretching mechanism.

Figures 5(*c*) and 5(*d*) plot $\varepsilon_{max}/\varepsilon_{app}$ as a function of arc angle α for narrow serpentines ($w/R = 0.2$) and wide serpentines ($w/R = 1$), respectively. It is important to note that the effect of α is not monotonic. As α decreases, i.e., when serpentine shape goes from tortuous to straight, $\varepsilon_{max}/\varepsilon_{app}$ first increases and then decreases till it reaches 1 at $\alpha = -\pi/2$. If we draw green dashed lines at $\varepsilon_{max}/\varepsilon_{app} = 1$ in Figs. 5(*c*) and 5(*d*), it is striking that a significant portion of each curve is above 1, which indicates that serpentines in those shapes can lead to strain concentration instead of strain relieving and that the stretchability of those serpentines can be lower than their linear counterparts. Comparing Fig. 5(*c*) with Fig. 5(*d*), the effect of strain concentration is more significant in wider serpentines. Therefore, mechanics modeling is crucial to serpentine design and extra caution is required when designing less tortuous or wide serpentines as they may be even less stretchable than straight ribbons. Although all three types of solutions support the abovementioned generic conclusions, there is some significant deviation between CB and FEM solutions, especially for wide and short serpentines, as represented by the black dashed curve and black dots in Fig. 5(*d*). In comparison, elasticity solutions represented by solid curves are much closer to FEM results for all serpentine shapes.

More results of abnormal serpentines are offered in Figs. 5(*e*) and 5(*f*). Figure 5(*e*) plots the elasticity solution of the arc angle at peak strain α_p as the left axis and the value of peak strain $(\varepsilon_{max}/\varepsilon_{app})_p$ as the right axis versus w/R for different l/R. For the given ranges of serpentine shapes ($0.2 \le w/R \le 1$, $0 < l/R \le 3$), $(\varepsilon_{max}/\varepsilon_{app})_p$ can be as high as 2.9 at $w/R = 1$, $l/R = 0$, $\alpha = -77$ deg. In addition to the peak strain, it is also helpful to have curves that separate stretchable and nonstretchable serpentines. We use α_c to denote the critical arc angle below which $\varepsilon_{max}/\varepsilon_{app}$ gets beyond 1, i.e., the intersections between the curves and the green dashed lines in Figs. 5(*c*) and 5(*d*). Using the elasticity solution, Fig. 5(*f*) plots α_c as a function of w/R for different l/R, and representative serpentine shapes are drawn as insets labeled with their shape parameters $(w/R, l/R, \alpha)$. For serpentines with given arm length, e.g., $l/R = 1$, then as long as their $(w/R, \alpha)$ combination falls above the red curve, the $\varepsilon_{max}/\varepsilon_{app}$ of

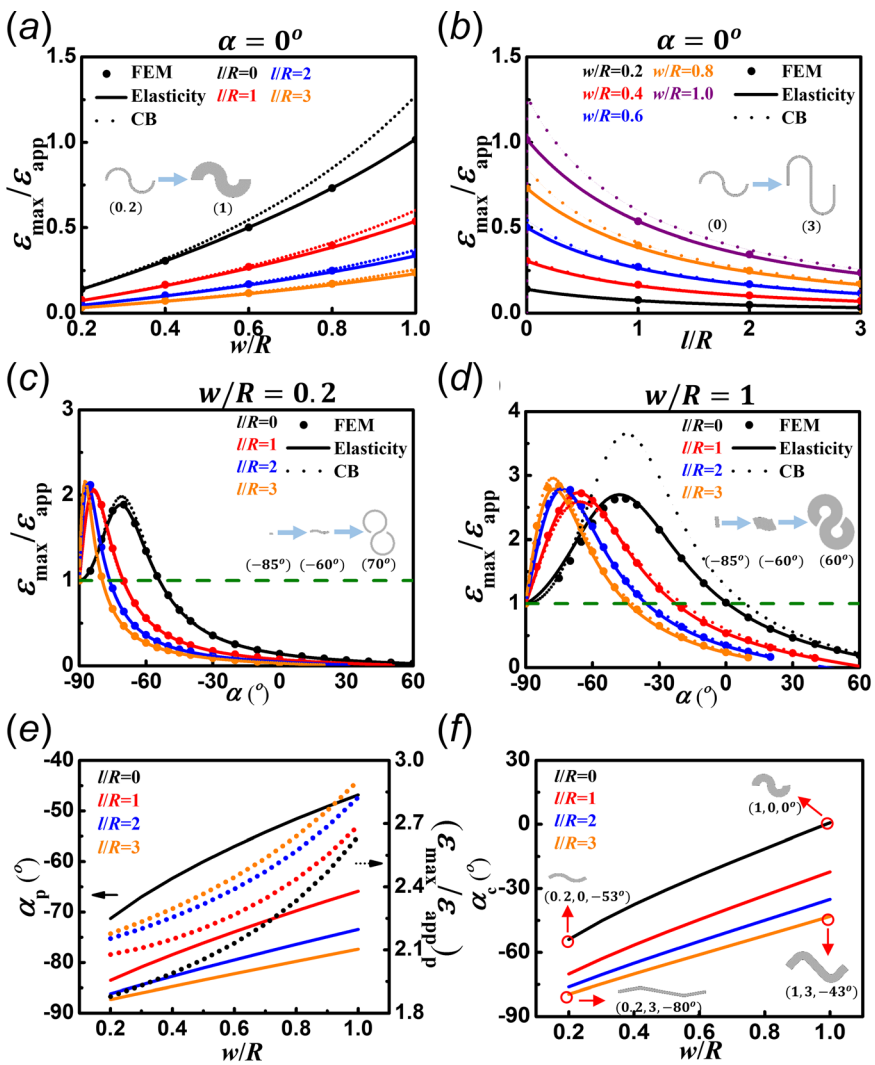

Fig. 5 Normalized maximum strain obtained by elasticity theory (solid curve), CB theory (dashed curve), and FEM (dot) when (*a*) and (*b*) $\alpha = 0$, (*c*) $w/R = 0.2$, and (*d*) $w/R = 1$. (*e*) Arc angle at peak strain α_p (left axis) and value of peak strain $(\varepsilon_{max}/\varepsilon_{app})_p$ (right axis) plotted as functions of w/R. (*f*) Critical arc angle α_c above which $\varepsilon_{max}/\varepsilon_{app}<1$ plotted as a function of w/R for various l/R.

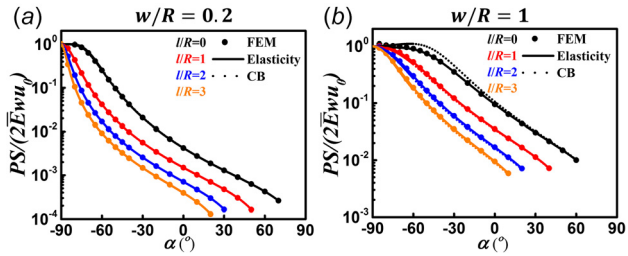

Fig. 6 Normalized effective stiffness of serpentines $PS/(2\bar{E}wu_0)$ plotted for (*a*) narrow serpentines ($w/R = 0.2$) and (*b*) wide serpentines ($w/R = 1$)

this serpentine is predicted to be less than 1, and hence more stretchable than straight ribbons. Therefore, this plot can be used as a handy tool to determine whether certain serpentine shape would enhance stretchability.

3.2 Effective Stiffness of Serpentine Ribbons. Other than stretchability, effective stiffness is also an important property of serpentine ribbons since it reflects how "soft" the structure is. Figures 6(*a*) and 6(*b*) plot the effective stiffness of serpentine ribbons normalized by that of a straight ribbon in semi-log scales for narrow serpentines ($w/R = 0.2$) and wide serpentines ($w/R = 1$), respectively. It is obvious that the elasticity solution finds good agreement with FEM results for both narrow and wide serpentines while the CB solution works very well for narrow serpentines but shows slight deviation for wide serpentines. Both figures suggest that the normalized effective stiffness are always smaller than 1, which indicates that serpentines are always "softer" than their linear counterparts, even if they are not always more stretchable. All three dimensionless geometric parameters have monotonic effect

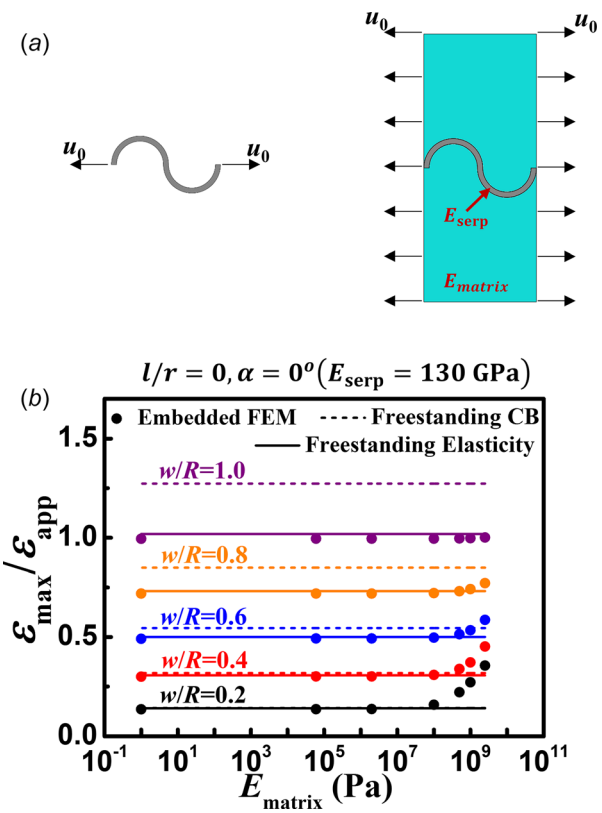

Fig. 7 (*a*) Boundary conditions for plane strain freestanding and polymer embedded serpentines. (*b*) $\varepsilon_{max}/\varepsilon_{app}$ as a function of the matrix modulus E_{matrix}: dots are FEM results of embedded serpentines whereas solid and dashed lines are elasticity and CB solutions, respectively, of freestanding serpentines.

on the effective stiffness, i.e., serpentine ribbons are softer when they have smaller w/R, larger l/R, and larger α. In fact, the reduction of effective stiffness can be orders of magnitude, which enables the creation of tissue-like electronics out of inorganic semiconductors and conductors whose intrinsic stiffness is several orders higher than that of bio-tissues.

3.3 Nonbuckling Serpentine Ribbons Embedded in Polymer Matrix. So far, we have presented the stretchability and effective stiffness of freestanding nonbuckling serpentine ribbons. When serpentine ribbons are embedded in a polymer matrix and then stretched [16,36], we expect that the strain would exceed that in freestanding serpentines due to the constraint from the polymer matrix. We performed 2D plane strain FEM of a unit cell to reveal the strain in embedded serpentines when u_0 is applied at each end to pull the polymer matrix, as illustrated in Fig. 7(*a*). Adopting the same definition of ε_{app} in Eq. (2), Fig. 7(*b*) plots the FEM solution of $\varepsilon_{max}/\varepsilon_{app}$ as a function of the Young's modulus of the polymer matrix E_{matrix} in dots, with the serpentine Young's modulus fixed to be $E_{serp} = 130$ GPa, a representative modulus for inorganic electronic materials. For comparison, we also plot the CB solutions as dashed lines and elasticity solutions as solid lines for freestanding nonbuckling serpentines in Fig. 7(*b*), which are flat because they are independent of E_{matrix}. It is interesting to discover that when $E_{matrix} < 100$ MPa, the FEM results of embedded serpentines fall right on the elasticity solutions of freestanding serpentines, which suggests that the soft polymer matrix has negligible effects on the deformation of polymer-embedded stiff, nonbuckling serpentine ribbons. Fortunately, the Young's moduli of many popular stretchable polymers such as 10:1 Sylgard 184 PDMS (polydimethylsiloxane) and Ecoflex are well below 100 MPa and therefore our analytical solutions to the freestanding serpentines are still applicable when the serpentines are embedded in such stretchable polymers. When the polymer becomes very stiff, e.g., polyimide has a Young's modulus of 2.5 GPa, Fig. 7(*b*) suggests that the elasticity solutions are still close to the FEM results for wide serpentines ($w/R \geq 0.8$) whereas significant deviation exists in narrower serpentines. This can be attributed to the high effective stiffness of wide serpentines as shown in Fig. 6(*b*).

4 Conclusions

We have derived full-field elasticity solutions to freestanding, nonbuckling serpentine ribbons defined by three independent, dimensionless geometric parameters. We have demonstrated that weak boundary conditions are sufficient for solving Airy stress functions except when the serpentine's total curve length approaches the ribbon width. Slightly modified weak boundary conditions have been proposed to resolve this difficulty. Our elasticity solutions to the maximum strain and effective stiffness are compared with FEM results and previously derived CB theory. The elasticity solution finds good agreement with FEM results for all serpentine shapes whereas the CB theory is only applicable to narrow serpentines. An important conclusion is that serpentines are not always more stretchable than their linear counterparts but they are always softer, easily by orders of magnitude. We have also studied the effect of polymer matrix on serpentine deformation and found out that our elasticity solution for freestanding nonbuckling serpentines are also applicable to serpentines with large effective stiffness embedded in soft polymer matrix such as elastomers.

Acknowledgment

This work was supported by the AFOSR Young Investigator Program under Grant No. FA9550-15-1-0112 managed by Dr. Byung-Lip (Les) Lee, and the NSF CMMI award under Grant No. 1509767. N.L. is thankful to the 3M Non-Tenured Faculty Award. S.Y. and S.Q. acknowledge the John and Mary Wheeler endowed graduate fellowship awarded by the Cockrell School of Engineering at the University of Texas at Austin.

Appendix

Stress fields in the arc

$$\begin{cases} \boldsymbol{\sigma_{rr}} = \dfrac{AP\left(\left(\frac{r}{a}\right)^2-1\right)\left(\left(\frac{r}{b}\right)^2-1\right)\cos(\theta)}{r^3} \\ \qquad + \dfrac{2BP\left(l\cos(\beta)-(a+b+2c)\sin(\beta)\right)\left(\left(1-\left(\frac{r}{b}\right)^2\right)\ln(a)-\left(1-\left(\frac{r}{a}\right)^2\right)\ln(b)+\left(\left(\frac{r}{b}\right)^2-\left(\frac{r}{a}\right)^2\right)\ln(r)\right)}{r^2} \\ \boldsymbol{\sigma_{\theta\theta}} = -\dfrac{AP\left(1+\left(\frac{r}{a}\right)^2+\left(\frac{r}{b}\right)^2-3\left(\frac{r}{a}\right)^2\left(\frac{r}{b}\right)^2\right)\cos(\theta)}{r^3} \\ \qquad - \dfrac{2BP\left(l\cos(\beta)-(a+b+2c)\sin(\beta)\right)\left(\left(1+\left(\frac{r}{b}\right)^2\right)\ln(a)-\left(1+\left(\frac{r}{a}\right)^2\right)\ln(b)-\left(\left(\frac{r}{b}\right)^2-\left(\frac{r}{a}\right)^2\right)(1+\ln(r))\right)}{r^2} \\ \boldsymbol{\sigma_{r\theta}} = \dfrac{AP\left(\left(\frac{r}{a}\right)^2-1\right)\left(\left(\frac{r}{b}\right)^2-1\right)\sin(\theta)}{r^3} \end{cases} \tag{A1}$$

where

$$A = \frac{a^2b^2}{\left(-a^2+b^2+(a^2+b^2)\ln\left(\frac{a}{b}\right)\right)}, \quad B = \frac{a^2b^2}{\left(a^2-b^2+2ab\ln\left(\frac{a}{b}\right)\right)\left(a^2-b^2+2ab\ln\left(\frac{b}{a}\right)\right)} \tag{A2}$$

Stress fields in the arm

$$\begin{cases} \sigma_{xx} = -\dfrac{P\left(6(1-2x)y\cos(\beta)\right)+\left((a-b)^2-12cy\right)\sin(\beta))}{(a-b)^3} \\ \sigma_{yy} = 0 \\ \sigma_{xy} = \dfrac{3P\left((a-b)^2-4y^2\right)\cos(\beta)}{2(a-b)^3} \end{cases} \tag{A3}$$

Strain fields can be obtained from the stress fields by using linear elastic constitutive law.

Displacement fields in the arc

$$u_r = \frac{P}{2\bar{E}}\left(\begin{array}{c} \dfrac{A}{r^2}\cos(\theta)\left(\dfrac{r^4}{a^2b^2}(1-3\bar{\nu})-(1+\bar{\nu})+2\left(\dfrac{r^2}{a^2}+\dfrac{r^2}{b^2}\right)(-1+\bar{\nu})\ln(r)\right) \\ +4B\dfrac{-l\cos(\beta)+(a+b+2c)\sin(\beta)}{r}\left(\left(-\dfrac{r^2}{b^2}(-1+\bar{\nu})+(1+\bar{\nu})\right)\ln(a)\right. \\ \left.-\left(-\dfrac{r^2}{a^2}(-1+\bar{\nu})+(1+\bar{\nu})\right)\ln(b)+\left(\dfrac{r^2}{b^2}-\dfrac{r^2}{a^2}\right)\left(1+(-1+\bar{\nu})\ln(r)\right)\right) \\ -4A\theta\sin(\theta)\left(\dfrac{1}{a^2}+\dfrac{1}{b^2}\right) \end{array}\right)$$

$$u_\theta = \frac{P}{2\bar{E}}\left(\begin{array}{c} 8Br\theta\left(\dfrac{1}{b^2}-\dfrac{1}{a^2}\right)\left(l\cos(\beta)-(a+b+2c)\sin(\beta)\right)-4A\theta\cos(\theta)\left(\dfrac{1}{a^2}+\dfrac{1}{b^2}\right) \\ +A\sin(\theta)\left(\left(\dfrac{2}{a^2}+\dfrac{2}{b^2}-\dfrac{1}{r^2}\right)(1+\bar{\nu})+\dfrac{r^2}{a^2b^2}(5+\bar{\nu})-\left(\dfrac{2}{a^2}+\dfrac{2}{b^2}\right)(-1+\bar{\nu})\ln(r)\right) \end{array}\right) \tag{A4}$$

Displacement fields in the arm

$$u_x = \frac{P\cos(\beta)}{2(a-b)^3\bar{E}}\left(-4d^3(-1+\bar{\nu}) + 12(d^2 - \mathrm{lx} + x^2)y \right.$$
$$\left. -4(2+\bar{\nu})y^3 + 3(a-b)^2(1+\bar{\nu})(d+y)\right)$$
$$-\frac{Px\sin(\beta)}{(a-b)\bar{E}} - \frac{12cy\sin(\beta)}{(a-b)^3\bar{E}} - \phi(d+y)$$

$$u_y = \frac{P\cos(\beta)}{2(a-b)^3\bar{E}}\left(-6d^2(l\bar{\nu}+2x)\right.$$
$$\left. +x\left(3(a-b)^2(1+\bar{\nu}) + 6\mathrm{lx} - 4x^2\right) + 6\bar{\nu}(l-2x)y^2\right) \qquad \text{(A5)}$$
$$+\frac{P\bar{\nu}(d+y)\sin(\beta)}{(a-b)\bar{E}} - \frac{6cP\left(-d^2\bar{\nu} + x^2 + \bar{\nu}y^2\right)\sin(\beta)}{(a-b)^3\bar{E}} + \phi x$$

where $\bar{E} = E/(1-\nu^2)$ is the plane strain modulus and $\bar{\nu} = \nu/(1-\nu)$ is the plane strain Poisson's ratio.

References

[1] Rogers, J. A., Someya, T., and Huang, Y. G., 2010, "Materials and Mechanics for Stretchable Electronics," Science, **327**(5973), pp. 1603–1607.

[2] Suo, Z. G., 2012, "Mechanics of Stretchable Electronics and Soft Machines," MRS Bull., **37**(3), pp. 218–225.

[3] Hammock, M. L., Chortos, A., Tee, B. C. K., Tok, J. B. H., and Bao, Z. A., 2013, "25th Anniversary Article: The Evolution of Electronic Skin (E-Skin): A Brief History, Design Considerations, and Recent Progress," Adv. Mater., **25**(42), pp. 5997–6037.

[4] Song, Y. M., Xie, Y. Z., Malyarchuk, V., Xiao, J. L., Jung, I., Choi, K. J., Liu, Z. J., Park, H., Lu, C. F., Kim, R. H., Li, R., Crozier, K. B., Huang, Y. G., and Rogers, J. A., 2013, "Digital Cameras With Designs Inspired by the Arthropod Eye," Nature, **497**(7447), pp. 95–99.

[5] Kim, D. H., Lu, N. S., Ma, R., Kim, Y. S., Kim, R. H., Wang, S. D., Wu, J., Won, S. M., Tao, H., Islam, A., Yu, K. J., Kim, T. I., Chowdhury, R., Ying, M., Xu, L. Z., Li, M., Chung, H. J., Keum, H., McCormick, M., Liu, P., Zhang, Y. W., Omenetto, F. G., Huang, Y. G., Coleman, T., and Rogers, J. A., 2011, "Epidermal Electronics," Science, **333**(6044), pp. 838–843.

[6] Kang, S. K., Murphy, R. K. J., Hwang, S. W., Lee, S. M., Harburg, D. V., Krueger, N. A., Shin, J. H., Gamble, P., Cheng, H. Y., Yu, S., Liu, Z. J., McCall, J. G., Stephen, M., Ying, H. Z., Kim, J., Park, G., Webb, R. C., Lee, C. H., Chung, S. J., Wie, D. S., Gujar, A. D., Vemulapalli, B., Kim, A. H., Lee, K. M., Cheng, J. J., Huang, Y. G., Lee, S. H., Braun, P. V., Ray, W. Z., and Rogers, J. A., 2016, "Bioresorbable Silicon Electronic Sensors for the Brain," Nature, **530**(7588), pp. 71–76.

[7] Lipomi, D. J., Tee, B. C. K., Vosgueritchian, M., and Bao, Z. N., 2011, "Stretchable Organic Solar Cells," Adv. Mater, **23**(15), pp. 1771–1775.

[8] Xu, S., Zhang, Y. H., Cho, J., Lee, J., Huang, X., Jia, L., Fan, J. A., Su, Y. W., Su, J., Zhang, H. G., Cheng, H. Y., Lu, B. W., Yu, C. J., Chuang, C., Kim, T. I., Song, T., Shigeta, K., Kang, S., Dagdeviren, C., Petrov, I., Braun, P. V., Huang, Y. G., Paik, U., and Rogers, J. A., 2013, "Stretchable Batteries With Self-Similar Serpentine Interconnects and Integrated Wireless Recharging Systems," Nat. Commun., **4**, p. 1543.

[9] Shield, T. W., Kim, K. S., and Shield, R. T., 1994, "The Buckling of an Elastic Layer Bonded to an Elastic Substrate in Plane-Strain," ASME J. Appl. Mech., **61**(2), pp. 231–235.

[10] Bowden, N., Brittain, S., Evans, A. G., Hutchinson, J. W., and Whitesides, G. M., 1998, "Spontaneous Formation of Ordered Structures in Thin Films of Metals Supported on an Elastomeric Polymer," Nature, **393**(6681), pp. 146–149.

[11] Huang, R., and Suo, Z., 2002, "Instability of a Compressed Elastic Film on a Viscous Layer," Int. J. Solids Struct., **39**(7), pp. 1791–1802.

[12] Lacour, S. P., Wagner, S., Huang, Z. Y., and Suo, Z., 2003, "Stretchable Gold Conductors on Elastomeric Substrates," Appl. Phys. Lett., **82**(15), pp. 2404–2406.

[13] Khang, D. Y., Jiang, H. Q., Huang, Y., and Rogers, J. A., 2006, "A Stretchable Form of Single-Crystal Silicon for High-Performance Electronics on Rubber Substrates," Science, **311**(5758), pp. 208–212.

[14] Qi, Y., Kim, J., Nguyen, T. D., Lisko, B., Purohit, P. K., and McAlpine, M. C., 2011, "Enhanced Piezoelectricity and Stretchability in Energy Harvesting Devices Fabricated From Buckled PZT Ribbons," Nano Lett., **11**(3), pp. 1331–1336.

[15] Wang, Y., Yang, R., Shi, Z. W., Zhang, L. C., Shi, D. X., Wang, E., and Zhang, G. Y., 2011, "Super-Elastic Graphene Ripples for Flexible Strain Sensors," ACS Nano, **5**(5), pp. 3645–3650.

[16] Gray, D. S., Tien, J., and Chen, C. S., 2004, "High-Conductivity Elastomeric Electronics," Adv. Mater., **16**(5), pp. 393–397.

[17] Li, T., Suo, Z. G., Lacour, S. P., and Wagner, S., 2005, "Compliant Thin Film Patterns of Stiff Materials as Platforms for Stretchable Electronics," J. Mater. Res., **20**(12), pp. 3274–3277.

[18] Brosteaux, D., Axisa, F., Gonzalez, M., and Vanfleteren, J., 2007, "Design and Fabrication of Elastic Interconnections for Stretchable Electronic Circuits," IEEE Electron. Device Lett., **28**(7), pp. 552–554.

[19] Kim, D. H., Song, J. Z., Choi, W. M., Kim, H. S., Kim, R. H., Liu, Z. J., Huang, Y. Y., Hwang, K. C., Zhang, Y. W., and Rogers, J. A., 2008, "Materials and Noncoplanar Mesh Designs for Integrated Circuits With Linear Elastic Responses to Extreme Mechanical Deformations," Proc. Natl. Acad. Sci. U.S.A., **105**(48), pp. 18675–18680.

[20] Hsu, Y. Y., Gonzalez, M., Bossuyt, F., Axisa, F., Vanfleteren, J., and De Wolf, I., 2009, "In Situ Observations on Deformation Behavior and Stretching-Induced Failure of Fine Pitch Stretchable Interconnect," J. Mater. Res., **24**(12), pp. 3573–3582.

[21] Kim, D. H., Lu, N. S., Ghaffari, R., Kim, Y. S., Lee, S. P., Xu, L. Z., Wu, J. A., Kim, R. H., Song, J. Z., Liu, Z. J., Viventi, J., de Graff, B., Elolampi, B., Mansour, M., Slepian, M. J., Hwang, S., Moss, J. D., Won, S. M., Huang, Y. G., Litt, B., and Rogers, J. A., 2011, "Materials for Multifunctional Balloon Catheters With Capabilities in Cardiac Electrophysiological Mapping and Ablation Therapy," Nat. Mater., **10**(4), pp. 316–323.

[22] Kim, R. H., Bae, M. H., Kim, D. G., Cheng, H. Y., Kim, B. H., Kim, D. H., Li, M., Wu, J., Du, F., Kim, H. S., Kim, S., Estrada, D., Hong, S. W., Huang, Y. G., Pop, E., and Rogers, J. A., 2011, "Stretchable, Transparent Graphene Interconnects for Arrays of Microscale Inorganic Light Emitting Diodes on Rubber Substrates," Nano Lett., **11**(9), pp. 3881–3886.

[23] Ma, T., Wang, Y., Tang, R., Yu, H., and Jiang, H., 2013, "Pre-Patterned ZnO Nanoribbons on Soft Substrates for Stretchable Energy Harvesting Applications," J. Appl. Phys., **113**(20), p. 204503.

[24] Yang, S., Ng, E., and Lu, N., 2015, "Indium Tin Oxide (ITO) Serpentine Ribbons on Soft Substrates Stretched Beyond 100%," Extreme Mech. Lett., **2**, pp. 37–45.

[25] Lu, N. S., Lu, C., Yang, S. X., and Rogers, J., 2012, "Highly Sensitive Skin-Mountable Strain Gauges Based Entirely on Elastomers," Adv. Funct. Mater., **22**(19), pp. 4044–4050.

[26] Fan, J. A., Yeo, W. H., Su, Y. W., Hattori, Y., Lee, W., Jung, S. Y., Zhang, Y. H., Liu, Z. J., Cheng, H. Y., Falgout, L., Bajema, M., Coleman, T., Gregoire, D., Larsen, R. J., Huang, Y. G., and Rogers, J. A., 2014, "Fractal Design Concepts for Stretchable Electronics," Nat. Commun., **5**, p. 3266.

[27] Zhang, Y., Fu, H., Xu, S., Fan, J. A., Hwang, K.-C., Jiang, J., Rogers, J. A., and Huang, Y., 2014, "A Hierarchical Computational Model for Stretchable Interconnects With Fractal-Inspired Designs," J. Mech. Phys. Solids, **72**, pp. 115–130.

[28] Son, D., Lee, J., Lee, D. J., Ghaffari, R., Yun, S., Kim, S. J., Lee, J. E., Cho, H. R., Yoon, S., Yang, S. X., Lee, S., Qiao, S. T., Ling, D. S., Shin, S., Song, J. K., Kim, J., Kim, T., Lee, H., Kim, J., Soh, M., Lee, N., Hwang, C. S., Nam, S., Lu, N. S., Hyeon, T., Choi, S. H., and Kim, D. H., 2015, "Bioresorbable Electronic Stent Integrated With Therapeutic Nanoparticles for Endovascular Diseases," ACS Nano, **9**(6), pp. 5937–5946.

[29] Lanzara, G., Salowitz, N., Guo, Z. Q., and Chang, F. K., 2010, "A Spider-Web-Like Highly Expandable Sensor Network for Multifunctional Materials," Adv. Mater., **22**(41), pp. 4643–4648.

[30] Liu, L., and Lu, N., 2016, "Variational Formulations, Instabilities and Critical Loadings of Space Curved Beams," Int. J. Solids Struct., **87**, pp. 48–60.

[31] Zhang, Y. H., Xu, S., Fu, H. R., Lee, J., Su, J., Hwang, K. C., Rogers, J. A., and Huang, Y. G., 2013, "Buckling in Serpentine Microstructures and Applications in Elastomer-Supported Ultra-Stretchable Electronics With High Areal Coverage," Soft Matter, **9**(33), pp. 8062–8070.

[32] Fan, Z. C., Zhang, Y. H., Ma, Q., Zhang, F., Fu, H. R., Hwang, K. C., and Huang, Y. G., 2016, "A Finite Deformation Model of Planar Serpentine Interconnects for Stretchable Electronics," Int. J. Solids Struct., **91**, pp. 46–54.

[33] Zhang, Y., Fu, H., Su, Y., Xu, S., Cheng, H., Fan, J. A., Hwang, K.-C., Rogers, J. A., and Huang, Y., 2013, "Mechanics of Ultra-Stretchable Self-Similar Serpentine Interconnects," Acta Mater., **61**(20), pp. 7816–7827.

[34] Su, Y., Wang, S., Huang, Y., Luan, H., Dong, W., Fan, J. A., Yang, Q., Rogers, J. A., and Huang, Y., 2015, "Elasticity of Fractal Inspired Interconnects," Small, **11**(3), pp. 367–373.

[35] Hsu, Y. Y., Gonzalez, M., Bossuyt, F., Axisa, F., Vanfleteren, J., and DeWolf, I., 2010, "The Effect of Pitch on Deformation Behavior and the Stretching-Induced Failure of a Polymer-Encapsulated Stretchable Circuit," J. Micromech. Microeng., **20**(7), p. 075036.

[36] Hsu, Y. Y., Gonzalez, M., Bossuyt, F., Axisa, F., Vanfleteren, J., and De Wolf, I., 2011, "The Effects of Encapsulation on Deformation Behavior and Failure Mechanisms of Stretchable Interconnects," Thin Solid Films, **519**(7), pp. 2225–2234.

[37] Hsu, Y. Y., Gonzalez, M., Bossuyt, F., Vanfleteren, J., and De Wolf, I., 2011, "Polyimide-Enhanced Stretchable Interconnects: Design, Fabrication, and Characterization," IEEE Trans. Electron. Devices, **58**(8), pp. 2680–2688.

[38] Yang, S., Su, B., Bitar, G., and Lu, N., 2014, "Stretchability of Indium Tin Oxide (ITO) Serpentine Thin Films Supported by Kapton Substrates," Int. J. Fracture, **190**(1–2), pp. 99–110.

[39] Xu, R., Jang, K.-I., Ma, Y., Jung, H. N., Yang, Y., Cho, M., Zhang, Y., Huang, Y., and Rogers, J. A., 2014, "Fabric-Based Stretchable Electronics With Mechanically Optimized Designs and Prestrained Composite Substrates," Extreme Mech. Lett., **1**, pp. 120–126.

[40] Widlund, T., Yang, S. X., Hsu, Y. Y., and Lu, N. S., 2014, "Stretchability and Compliance of Freestanding Serpentine-Shaped Ribbons," Int. J. Solids Struct., **51**(23–24), pp. 4026–4037.

[41] Bandodkar, A. J., Jeerapan, I., You, J. M., Nunez-Flores, R., and Wang, J., 2016, "Highly Stretchable Fully-Printed CNT-Based Electrochemical Sensors and Biofuel Cells: Combining Intrinsic and Design-Induced Stretchability," Nano Lett., **16**(1), pp. 721–727.

[42] Yang, S., Chen, Y. C., Nicolini, L., Pasupathy, P., Sacks, J., Becky, S., Yang, R., Daniel, S., Chang, Y. F., Wang, P., Schnyer, D., Neikirk, D., and Lu, N., 2015, ""Cut-and-Paste" Manufacture of Multiparametric Epidermal Sensor Systems," Adv. Mater., **27**(41), pp. 6423–6430.